

Supplementary Information

Designed multifunctional polymeric nanomedicines to inform on long-term biodistribution and tumour accumulation at multiple length scales following aptamer conjugation

N. F. Fletcher,^a Z. H. Houston,^a J. D. Simpson,^a R. N. Veedu,^{b,c} and K. J. Thurecht^a

^a*Centre for Advanced Imaging (CAI), Australian Institute for Bioengineering and Nanotechnology (AIBN), The University of Queensland, Brisbane, QLD, 4072, Australia.
and ARC Centre of Excellence in Convergent BioNano Science and Technology*

^b*Centre for Comparative Genomics, Murdoch University, Perth, WA, 6150, Australia*

^c*Perron Institute for Neurological and Translational Science, Perth, WA, 6009*

Materials and methods

Materials

Azobis(isobutyronitrile) (AIBN), HEPES buffer, sodium carbonate, sodium bicarbonate and Evans Blue were purchased from Sigma Aldrich (USA).

1-(4-isothiocyanatophenyl)-3-[6,17-dihydroxy-7,10,18,21-tetraoxo-27-(N-acetylhydroxylamino)-6,11,17, 22- tetraazaheptaicosine] thiourea (p-SCN-Bn-Deferoxamine) was purchased from Macrocyclics (USA). Dibenzylcyclooctyne-Amine (DBCO-amine) was purchased from Jena Bioscience (Germany).

N-hexane, acetonitrile, dimethylsulfoxide, diethyl ether, ethanol and tetrahydrofuran (THF) were used dry where applicable and of reagent grade quality. Milli-Q water (18.2 mΩ/cm) was used throughout.

Monomers, poly(ethylene glycol) monomethyl ether methacrylate 475 (PEGMA) and ethylene glycol dimethacrylate (EGDMA) were filtered through basic alumina to remove radical inhibitors before use.

Phosphoramidites for oligonucleotide synthesis were purchased from Glen Research (USA).

Azido-RAFT chain transfer agent (3-azidopropyl 2-(((dodecylthio)carbonothioyl)thio)-2-methylpropanoate)¹ and Cy5.5 methacrylate² (Cy5.5-amine purchased from Lumiprobe (USA)) were synthesized in house as previously reported.

RNV66-DBCO synthesis procedure

RNV66 was prepared in-house on an Expedite 8909 DNA synthesiser via standard phosphoramidite chemistry in 1 μmol scale (Activator: 1H-tetrazole, oxidizing agent: Tetrahydrofuran/Water/Pyridine/Iodine = 90.54/9.05/0.41/0.43 (v/v/v/w)). For the 5'-DBCO-TEG phosphoramidites, the coupling time was prolonged to 15 minutes. Synthesized oligonucleotide was deprotected and cleaved from the solid support by treatment with NH₄OH at 55 °C overnight. The crude oligonucleotide was then desalted and purified by 20% denaturing polyacrylamide gel-electrophoresis (Figure S1)

Oligo name	Sequence (5'-3')
RNV66-DBCO	X TGT <u>GGG</u> GGT GGA CGG GCC <u>GGG</u> TAG <u>G</u> A
RNV66	TGT <u>GGG</u> GGT GGA CGG GCC <u>GGG</u> TAG <u>G</u> A

X: 5'-DBCO-TEG nucleotide; G: LNA-G nucleotide; all other nucleotides are DNA.

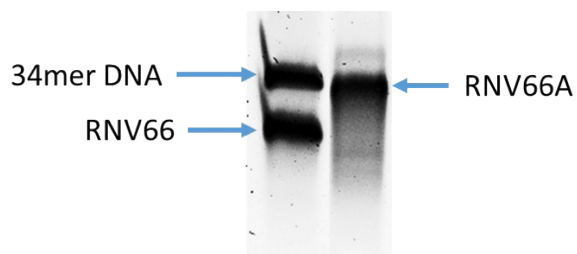


Figure S1 - Analysis of the purity of the synthesized AOs by 20% denaturing polyacrylamide gel electrophoresis

Characterisation Methods

Nuclear Magnetic Resonance analysis

All NMR experiments were undertaken on an AV3400 NMR spectrometer (Bruker (USA)). ¹H NMR spectra were collected in DMSO-d₆ for a minimum of 256 scans. [Size Exclusion Chromatography – Multiangle Laser Light Scattering studies](#)

SEC-MALLS analysis utilized a 1515 isocratic pump (Waters), a 717 auto sampler (Waters), Styragel HT 6E and Styragel HT 3 columns (Waters) and a 2414 differential refractive index detector (Wyatt) with THF as the eluent and a flow rate of 1 mL/min. To prevent interference from dye absorbance of GPC-MALLS laser (658 nm), 5 mg of **HBP1** was taken and bubbled with compressed air over silver to quench Cy5.5 ($\lambda_{\text{max}} = 684 \text{ nm}$) until dye absorbance was undetectable by UV-vis prior to analysis. Number-average molecular weight was then determined using a dn/dc of 0.060 as previously calculated for comparable PEGMA based HBPs.

UV-vis Spectroscopy

Samples were measured on a NanoDrop 2000c (Thermo Scientific) using a 1 cm path length cuvette. Known concentrations of **HBP1** were analysed to determine polymer chain size with respect to RAFT end-group ($\epsilon_{309 \text{ nm}} = 10566 \text{ M}^{-1} \text{ cm}^{-1}$ in acetonitrile). Similarly Cy5.5 incorporation was determined ($\epsilon_{684 \text{ nm}} = 209000 \text{ M}^{-1} \text{ cm}^{-1}$ in water) with respect to mass of polymer. Comparison to molecular weights determined by GPC-MALLS allowed calculation of number of chain ends and Cy5.5 per polymer.

Agarose gel electrophoresis

Gel electrophoresis utilized a 1% (w/v) agarose gel in TAE (Tris-acetate EDTA) buffer pre-mixed with 1X final SYBR safe stain (Thermo Fisher Scientific). Samples were loaded in 5% glycerol (v/v) and migration was effected by application of 100 V across the gel for 30 minutes using a Bio-Rad gel tank. The gel was then imaged on a Bruker In Vivo MS FX Pro imaging system using a 120 cm field-of-view with $\lambda_{\text{ex}} 480 \text{ nm}$ and $\lambda_{\text{em}} 600 \text{ nm}$ filters for SYBR stain, and $\lambda_{\text{ex}} 630 \text{ nm}$ and $\lambda_{\text{em}} 700 \text{ nm}$ filters for Cy5.5 imaging.

Dynamic light scattering and Zeta Potential measurements

Dynamic light scattering (DLS) was conducted on a DynaPro Plate Reader (Wyatt) using a 384-well black walled plate incubated at 25 °C. Polymer samples were prepared at 0.2 mg/mL in phosphate-

buffered saline and analysis comprised 5 repeat 10 second measurements, results from which were averaged.

Zeta potential measurements were conducted on a Zetasizer Nano (Malvern) using folded capillary zeta cells. Polymer samples were prepared at 0.2 mg/mL in phosphate-buffered saline and analysis comprised 3 repeat measurements, results from which were averaged.

Nanomedicine Synthesis

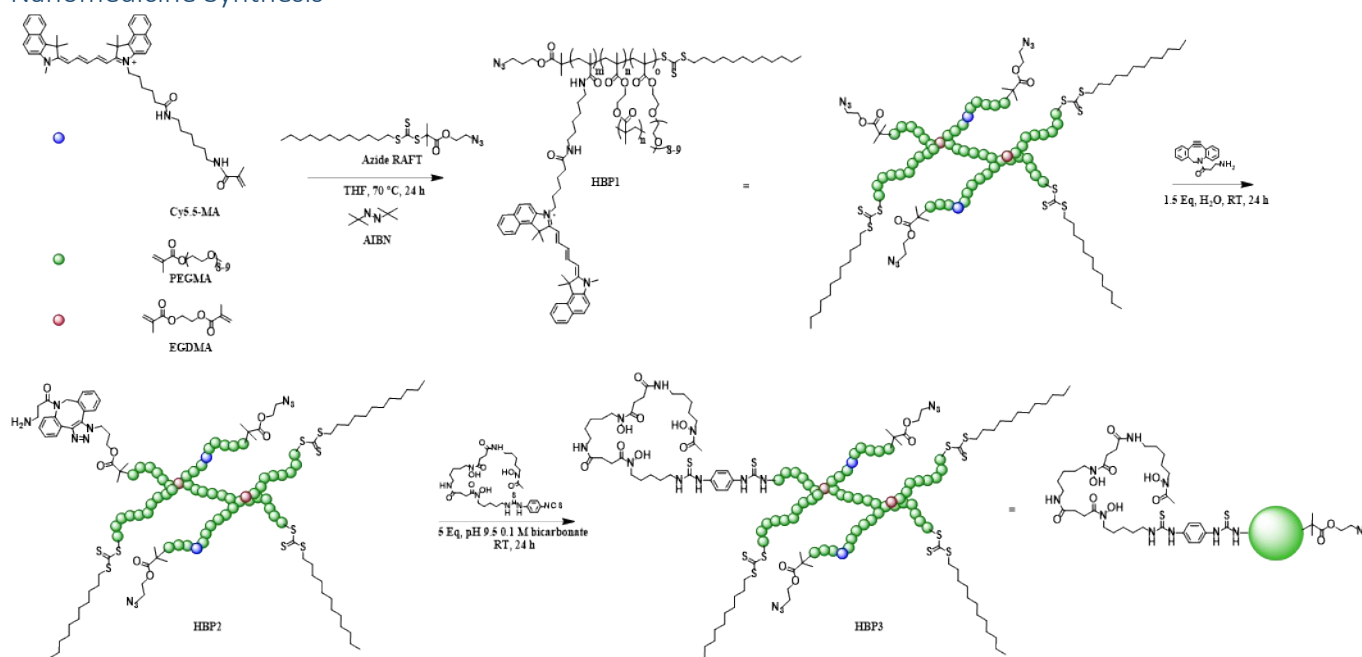


Figure S2 - Synthesis of a hyperbranched polymer core **HBP1** using RAFT polymerization and sequential modification to incorporate ^{89}Zr chelator desferoxamine to enable PET imaging (**HBP3**).

Polymeric Core Synthesis

Synthesis of hyperbranched polymer **HBP1** was based on previously described methods (Figure S2).²⁻⁴ In short, synthesis comprised the addition of PEGMA (193.8 mg, 0.408 mmol), EGDMA (12.2 mg, 0.061 mmol), Cy5.5 methacrylate (5 mg, 0.006 mmol), Azido-RAFT chain transfer agent (27.5 mg, 0.061 mmol) and AIBN (1 mg, 0.006 mmol) to a Schlenk tube. Reagents were dissolved in 390 μL THF, degassed with N_2 for 20 minutes, sealed and placed in a 70 °C oil bath for 24 hr. The products were then precipitated twice in 50 mL hexane:diethyl ether (90:10). The resulting blue-green oil was then dissolved in water/ethanol (80/20 (v/v)) and purified on an AKTA Prime Plus chromatography system (GE Healthcare Life Sciences) using two HiTrap desalting columns (GE Healthcare Life Sciences) in series with water/ethanol (80/20 (v/v)) as the eluent. The resulting polymer was characterized by ^1H NMR (Figure S3), SEC-MALLS and UV-vis.

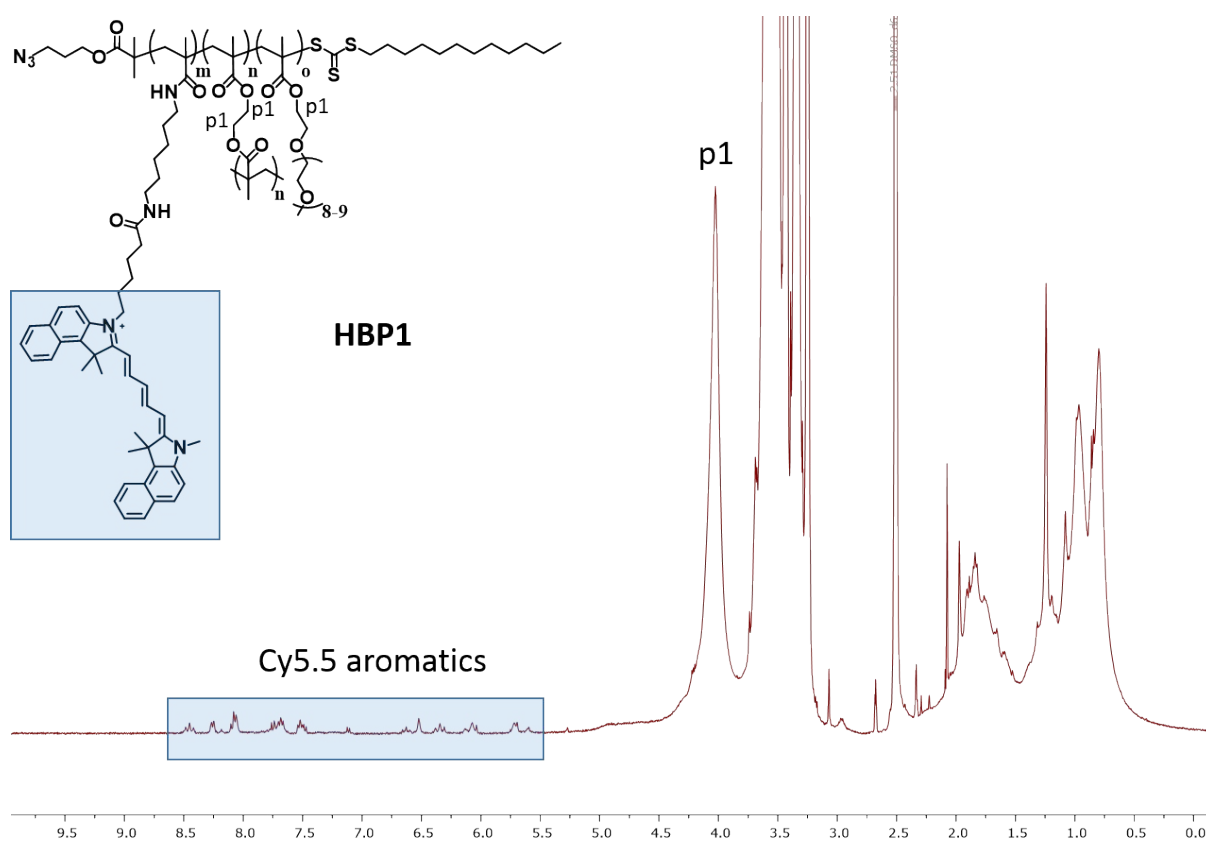


Figure S3 - Representative ^1H NMR spectra of hyperbranched polymer **HBP1**. The diagnostic resonance *p1* used for post-functionalization quantification is labelled and the aromatic resonances corresponding to Cy5.5 are highlighted in blue.

Modification of **HBP1** to give partially aminated **HBP2**

A portion of the azide chain ends of **HBP1** were then modified with DBCO-amine to give the partially aminated **HBP3**. **HBP1** (60 mg, 1.25 μmol) in 503 μL H_2O and DBCO-amine (0.52 mg, 1.9 μmol) in 74 μL DMSO were combined in a glass vial and stirred at room temperature overnight. The products were then dialysed against H_2O for 72 hours in a 3500 Da molecular weight cut-off Slide-A-Lyser dialysis cassette (Thermo Fisher Scientific). **HBP2** was then recovered, freeze dried and analysed by ^1H NMR (Figure S4) which shows an increase in ^1H integrations at 7.25-7.75 ppm compared to **HBP1** corresponding to DBCO aromatic protons.

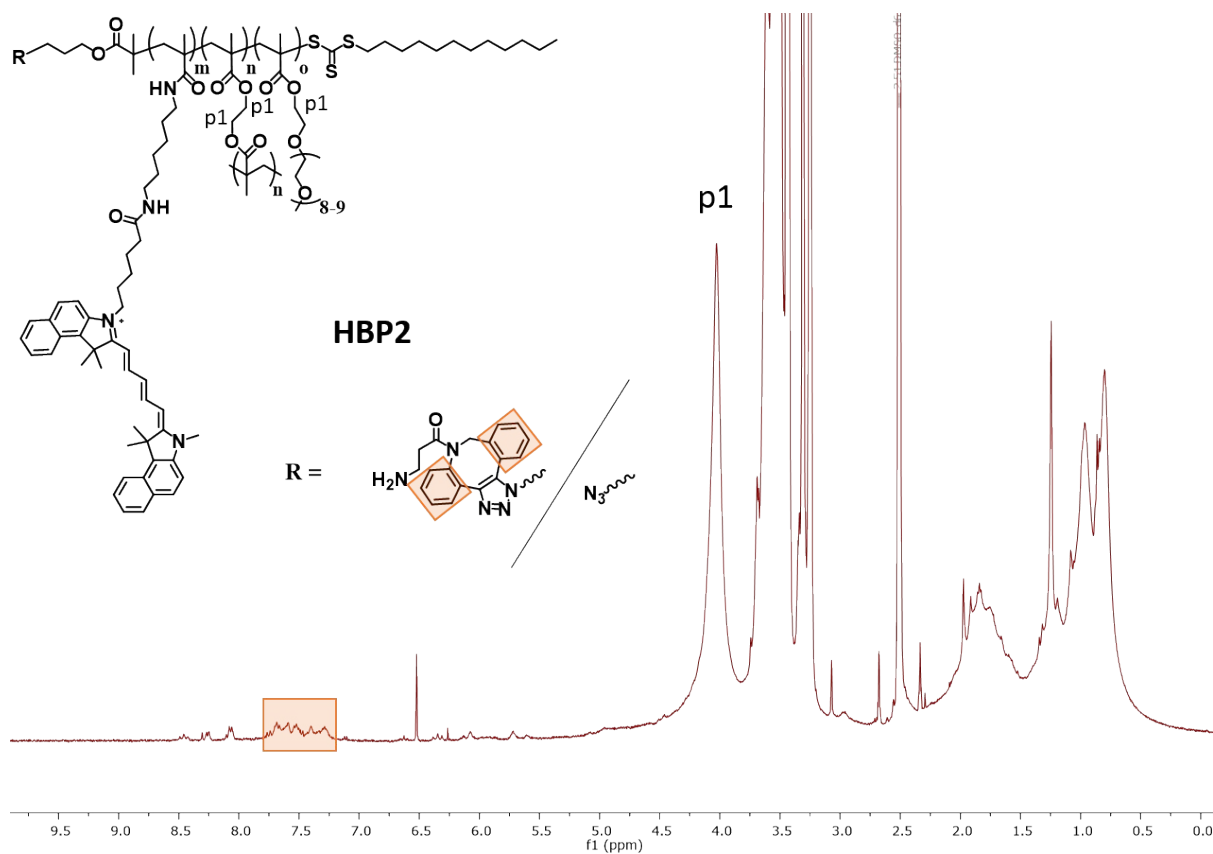


Figure S4 - Representative ^1H NMR spectra of hyperbranched polymer **HBP2**. Resonances corresponding to DBCO highlighted in orange.

Functionalization of **HBP2** with Desferoxamine to give **HBP3**

Amine chain ends of **HBP2** were functionalized with Des-isothiocyanate to give **HBP3**. Des-isothiocyanate (2.26 mg, 3 μmol) in 162 μL DMSO was added to a solution of **HBP2** (28.8 mg, 0.60 μmol) in 800 μL 0.1 M sodium bicarbonate pH 9.5. Stirred at room temperature overnight. The products were then dialysed against H_2O for 72 hours in a 3500 Da molecular weight cut-off Slide-A-Lyser dialysis cassette (Thermo Fisher Scientific). **HBP3** was then recovered, freeze dried and analysed by ^1H NMR (Figure S5) which shows characteristic resonances for desferoxamine. Integration of p2 compared to p1 shows attachment of 1.5 desferoxamine chelator per **HBP3**.

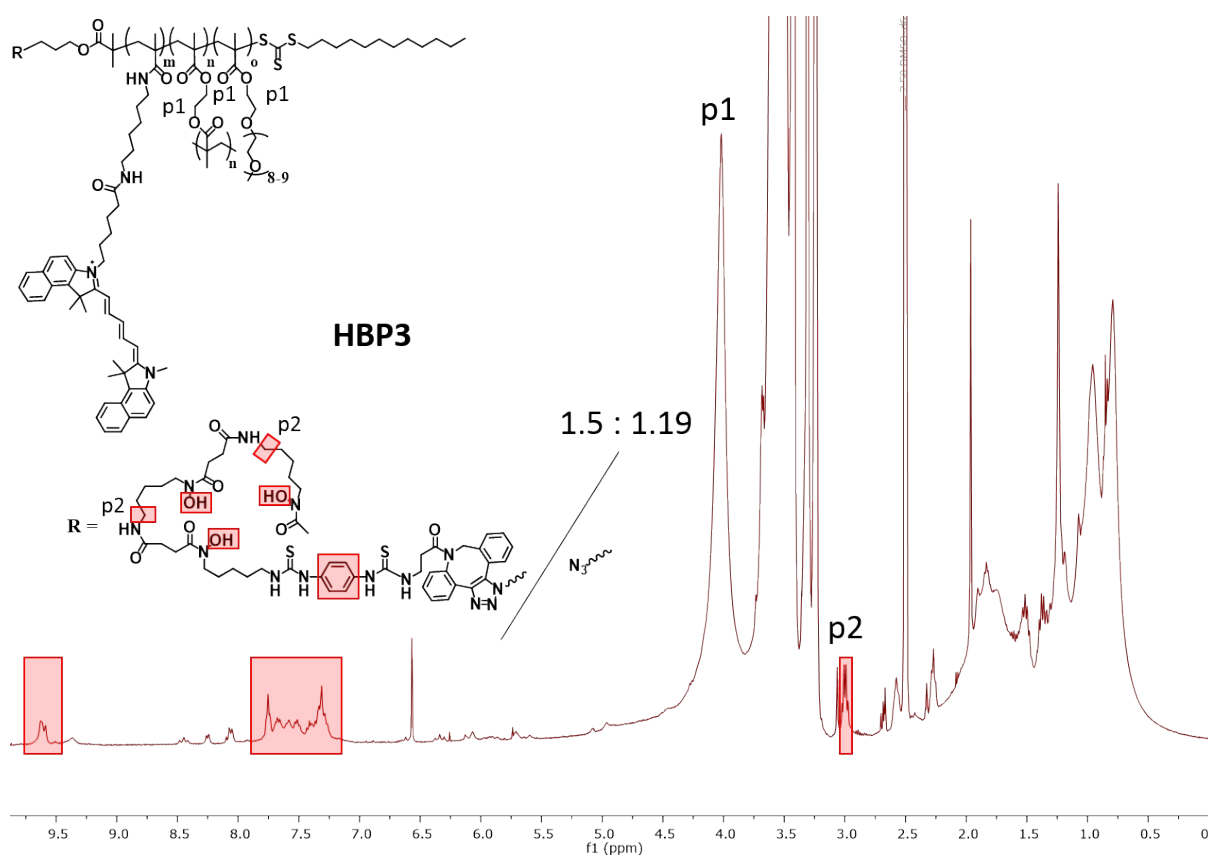


Figure S5 - Representative ^1H NMR spectra of hyperbranched polymer **HBP3**. Resonances corresponding to desferoxamine highlighted in red.

Aptamer conjugation to **HBP3**

DBCO-functionalized aptamer RNV66 (RNV66-DBCO) was conjugated to the remaining azide chain ends of **HBP3**. RNV66-DBCO (71.4 μg , 8.35 nmol) was added to **HBP3** (200 μg , 4.18 nmol) in 88 μL H_2O and stirred at room temperature overnight. Removal of free RNV66-DBCO was attempted using a 0.5 mL 30 K Amicon spin membrane with washes of ultrapure H_2O until no oligonucleotide absorbance at 260 nm was observed in the eluent (3X wash with 200 μL). Characterisation of conjugate formation *via* agarose gel electrophoresis confirmed attachment of the oligonucleotide to the HBP due to differing polymer mobility before and after conjugation as visualized by Cy5.5 fluorescence (Figure S6B). While **HBP3** alone showed no migration, the **HBP3-A** sample showed a prominent streaking effect through the gel. This streaking is a previously reported phenomenon of electrophoretic analysis of polymer-bio conjugations and is a result of both the polydispersity and globular shape of the polymer effecting migration through the gel matrix that is driven by the properties of the biomolecule.^{13, 14} Densitometry image analysis showed 56% of Cy5.5 fluorescence to be within the smear rather than the non-migrating band as for **HBP3**, suggesting at least 56% of **HBP3-A** to be aptamer functionalized. This is likely a lower limit of functionalization as the smear is partially continuous with the non-migrating band. SYBR Safe fluorescence imaging of oligonucleotide showed some free RNV66 to remain in the **HBP3-A** sample. Interestingly however, no SYBR signal was observed to correspond to the smear seen in the Cy5.5 image. This may be attributed to partial Förster resonance energy transfer (FRET) from the SYBR stain to Cy5.5 on the polymer (leading to subsequent quenching of the SYBR signal), as has previously been reported for SYBR dyes and NIR Cyanine dyes.¹⁵

As free aptamer was observed to remain following conjugation (Figure S6B) the material was washed on a 30K cutoff spin membrane repeatedly until no further absorbance at 260 nm was observed in

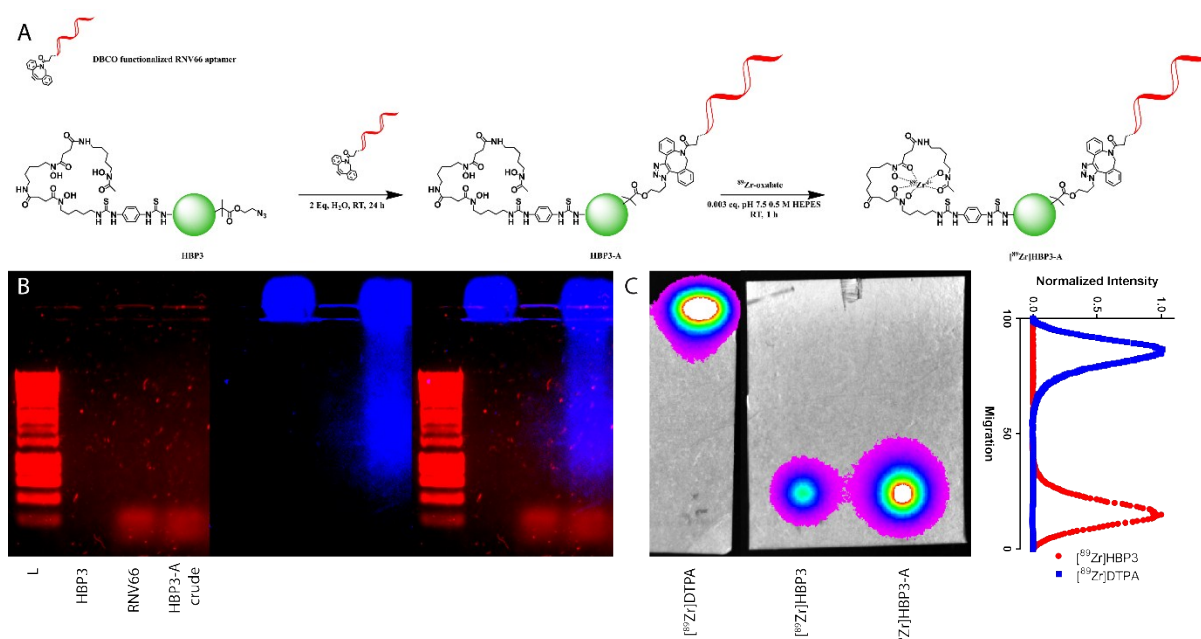


Figure S6 - Aptamer functionalization and ^{89}Zr labelling of hyperbranched polymer core **HBP3** for ^{89}Zr PET imaging of triple-negative breast cancer. A) Scheme illustrating synthetic steps to functionalize core **HBP3** with aptamer RNV66 to produce **HBP3-A** and subsequent ^{89}Zr labelling resulting in ^{89}Zr HBP3-A. B) Fluorescence imaging of agarose gels showing aptamer attachment to **HBP3** to give **HBP-A**. SYBR Safe staining shown in red and Cy5.5 shown in blue with overlaid image in third panel. C) Radiographic TLC and plotted distribution profile of ^{89}Zr chelated by DTPA, **HBP3** and **HBP3-A**.

the eluent. As the ^{89}Zr -PET imaging will be specific for the chelator functionalized nanomedicine **HBP3-A**, any residual free aptamer remaining after this washing step will not interfere with imaging results in determining the effect of aptamer conjugation on biodistribution and tumour-targeting efficacy.

^{89}Zr labelling

91 μL ^{89}Zr oxalate in 1 M oxalic acid (Perkin Elmer) was diluted with 78 μL 1 M Na_2CO_3 to neutralize pH. Nanomedicines **HBP3** and **HBP3-A** were prepared in 0.5 M HEPES (pH 7.5). 33 μL neutralized ^{89}Zr stock (approximately 15 MBq) was added to aliquots of each nanomedicine (146 μg) to give 300-fold excess of the nanomedicine to ^{89}Zr and labelling was allowed to proceed at room temperature for 1 hour. Samples were then buffer exchanged into phosphate-buffered saline using Zeba Spin Desalting Columns (7 kDa MWCO, Thermo Fisher Scientific). 1 μL samples of each solution were taken and spotted on thin layer chromatography paper (Agilent iTLC-SG Glass microfiber chromatography paper impregnated with silica gel) and run with 50 mM diethylenetriaminepentaacetic acid (DTPA) as the eluent. Control experiments were conducted to monitor the elution behaviour of unbound ^{89}Zr for quality control. Plates were then imaged on a Bruker In Vivo MS FX Pro imaging system using a radioisotopic phosphor screen.

Serum stability of ^{89}Zr -labelled nanomedicines

Samples of ^{89}Zr HBP3 were incubated in 50 % (v/v) foetal bovine serum (non-heat inactivated) at 37 $^\circ\text{C}$. Samples were taken at indicated times and TLC repeated as above with results shown in Figure S7.

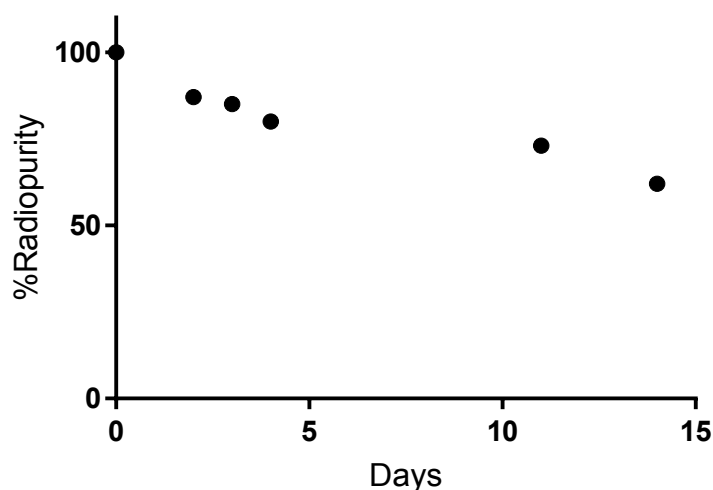


Figure S7 – Radiopurity of [⁸⁹Zr]HBP3 following incubation with serum

In vivo animal studies

Cells

MDA-MB-231 breast cancer cells were maintained in Roswell Park Memorial Institute (RPMI) medium supplemented with 10% (v/v) foetal bovine serum (heat inactivated, Bovogen), 100 U/mL Penicillin, 100 µg/mL Streptomycin and 2 mM L-glutamine.

Animals

All studies were in accordance with guidelines of the Animal Ethics Committee of The University of Queensland (UQ), and Australian Code for the Care and Use of Animals for Scientific Purposes. Mice were anaesthetised using 2 % isoflurane in O₂ for all injection and imaging procedures throughout. Female balb/c nu/nu mice (approximately 8 weeks of age) were injected (27 G needle, 50 µL PBS) with 5 x 10⁶ MDA-MB-231 cells in the mammary fat pad. Tumours were allowed to develop for 4 weeks before nanomedicine administration at which time they were approximately 5 mm in diameter.

Imaging

PET-CT

PET-CT imaging utilized a Siemens Inveon PET-CT scanner with physiological monitoring achieved using a respiratory probe (BioVet™ system, m2m Imaging, Australia). For dynamic biodistribution studies anaesthetized mice, with a cannulated tail vein, were positioned on the scanner bed and moved to the PET acquisition position. ⁸⁹Zr-labelled nanomedicine (**HBP3/HBP3-A**) was then injected (1-2 MBq activity per mouse, 200 µL phosphate buffered saline) and dynamic images acquired over the first 60 minutes following injection. Later PET scans were acquired at 1, 2, 3, 6 and 9 days after injection of the radiotracer, using 30 - 90 minute static acquisitions.

Following each PET acquisitions, micro-CT scans were acquired for anatomical co-registration. The CT images of the mice were acquired through an X-ray source with the voltage set to 80 kV and the current set to 500 µA. The scans were performed using 360° rotation with 120 rotation steps with a low magnification and a binning factor of four. The exposure time was 230 ms with an effective pixel size of 106 µm. The total CT scanning process took approximately 15 minutes. The CT images were reconstructed using Feldkamp reconstruction software (Siemens).

The PET Images were reconstructed using an ordered-subset expectation maximization (OSEM2D) algorithm and analysed using the Inveon Research Workplace software (IRW 4.1) (Siemens) which allows fusion of CT and PET images and definition of regions of interest (ROIs). CT and PET datasets of each individual animal were aligned using IRW software (Siemens) to ensure good overlap of the organs of interest. Three dimensional ROIs were placed within the whole body, as well as all the organs of interest, such as heart, kidney, lungs, bladder, liver, spleen, intestines and tumour, using morphologic CT information to delineate organs. Activity per voxel was converted to nci/cc using a conversion factor obtained by scanning a cylindrical phantom filled with a known activity of ^{89}Zr to account for PET scanner efficiency. Activity concentrations were then expressed as percent of the decay-corrected injected activity per cm^3 of tissue that can be approximate as percentage injected dose/g (%ID/g).

PET-MR

3 days after nanomedicine injection anaesthetized mice, with a cannulated tail vein, were placed in a combined MRI/PET system, comprising a 300mm bore 7T ClinScan, running Siemens VB17, and removable PET insert containing 3 rings of 16 detector blocks with 15×15 LSO crystals ($1.6 \times 1.6 \times 10\text{mm}$) per block, at the centre of the magnet bore operating under Siemens Inveon Acquisition Workplace (IAW) (Bruker, Germany). A 35 mm ID mouse body MRI RF coil inside the PET ring was used to acquire mouse images simultaneously with the PET acquisition.

^{89}Zr -PET data acquisition was performed for 60 min and fast localizer images and a 3D T1 weighted volumetric interpolated breath-hold examination (VIBE) sequence (TE 1.15, TR 15, FA 21, slice thickness $200 \mu\text{m}$) was acquired. Following initial MR imaging mice were injected with $25 \mu\text{l}$ Gadovist[®] and saline to give a total volume of $200 \mu\text{l}$. This volume was injected *via* a catheter inserted into the tail vein in a slow bolus injection. 15 minutes after Gadovist[®] injection the T1 weighted VIBE was repeated.

The PET data was reconstructed using dedicated PET reconstructed software developed by the University of Tübingen for the PET insert. PET images with a matrix of $128 \times 128 \times 89$ were reconstructed using the ordered-subset expectation maximization (OSEM2D) algorithm. MRI and PET datasets were aligned using IRW software (Siemens) using a transformation matrix generated using a phantom with known features.

Pharmacokinetics

Blood concentration of **HBP3-A** nanomedicine post injection was estimated by ROI analysis of PET images with heart signal used as a surrogate measure of blood concentration (Figure S8). This showed a biphasic blood elimination profile and was fit to a non-linear two phase decay following peak blood concentration, with an initial fast half-life of 1 hr and a slow half-life of approximately 13.4 hr (Figure S8). The initial fast clearance likely relates to tissue distribution following bolus administration, while the half-life of 13.4 hrs relates to the elimination phase of the material.

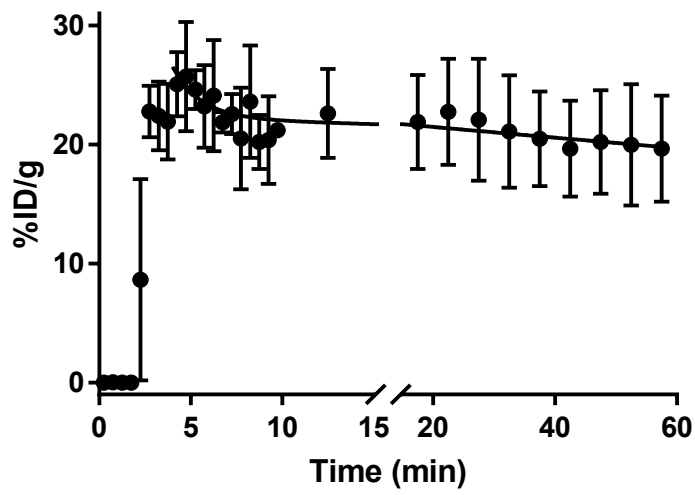


Figure S8 – Time-activity curve of the heart following injection of **HBP3-A** into tumour bearing mice. Line shows non-linear two phase decay fit following peak blood concentration. (n=3)

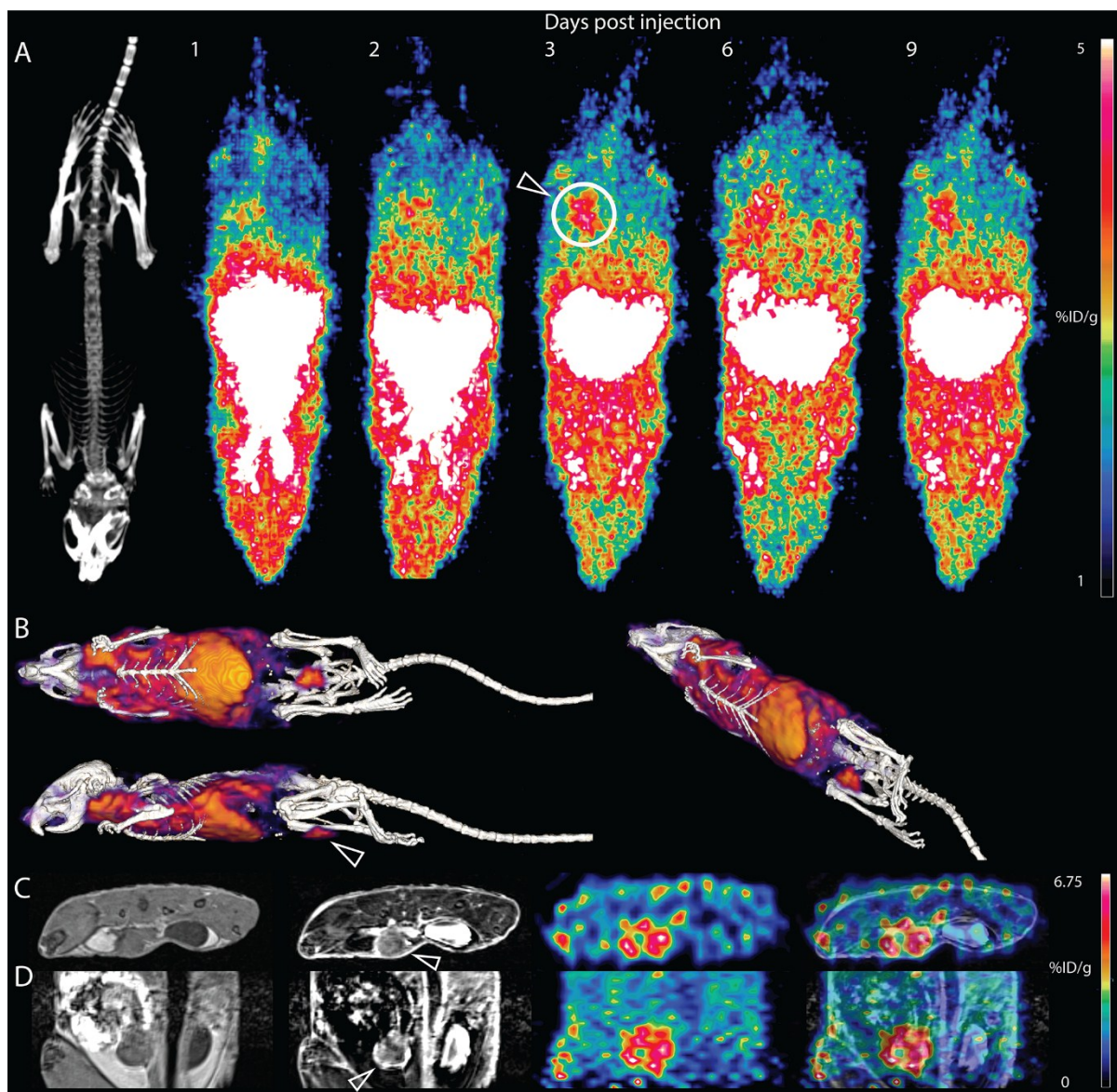


Figure S9 - PET-CT/MR imaging of ^{89}Zr -labelled aptamer-targeted nanomedicine $[^{89}\text{Zr}]\text{HBP3-A}$ in a TNBC xenograft model. A) MIPs of $[^{89}\text{Zr}]\text{HBP3-A}$ at indicated timepoints post injection. B) 3 orientations of 3D rendering of $[^{89}\text{Zr}]\text{HBP3-A}$ distribution at 3 days post injection. C) Coronal and D) sagittal PET-MRI image slices through tumour showing $[^{89}\text{Zr}]\text{HBP3-A}$ accumulation at 3 days post injection. Frames left to right show I) T_1 -weighted image, II) subtraction T_1 -weighted image following injection of gadolinium chelate highlighting highly perfused regions in white, III) PET image and IV) PET image overlaid with subtraction image from II). White arrowhead highlights tumour location in each image

^{89}Zr -PET imaging *in vivo* biodistribution

PET-CT images were acquired of mice at 1, 2, 3, 6 and 9 days post nanomedicine injection (Figure S9). Region-of-interest (ROI) analysis of images allowed for assessment of *in vivo* biodistribution at each time point (Figure S10).

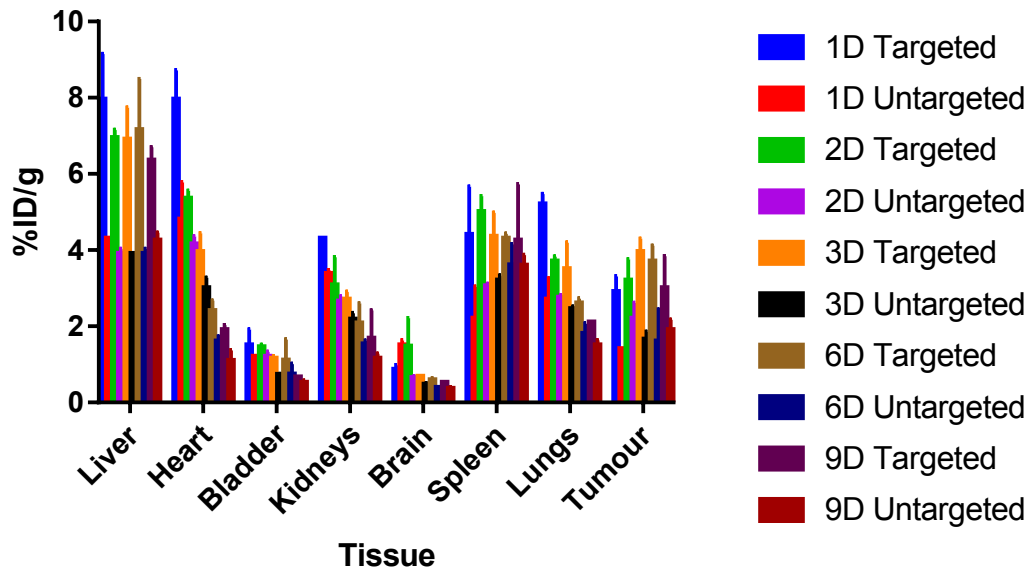


Figure S10 - Biodistribution of targeted and untargeted HBP as determined by ROI analysis of PET-CT images (n=2)

Figure S11 then shows plots for each tissue independently to allow better comparison of differences in tissue accumulation with time.

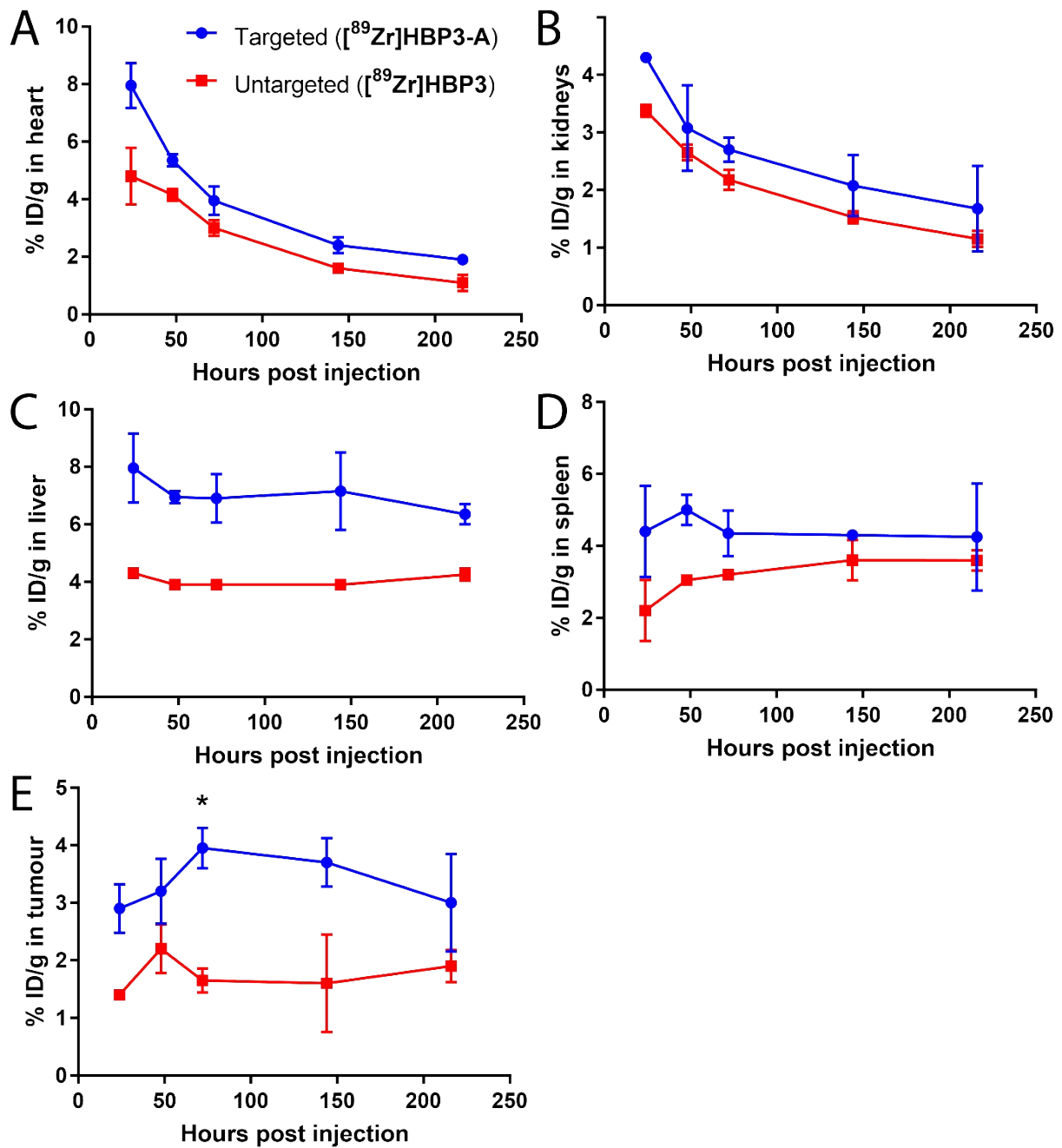


Figure S11. PET ROI analysis of *in vivo* tissue accumulation in TNBC xenograft model of untargeted ($[^{89}\text{Zr}]\text{HBP3}$) and targeted ($[^{89}\text{Zr}]\text{HBP3-A}$) nanomedicines. A-E) Plot of nanomedicine distribution over time for heart, kidneys, liver, spleen and tumour respectively,

Ex vivo analysis

Ex vivo biodistribution by λ scintillation counter

Following PET-CT image acquisition at 9 days post injection, animals were injected intravenously via the tail vein with Evans blue solution (29 G needle, 100 μL 1% (w/v) Evans blue in phosphate buffered saline) before euthanasia by cervical dislocation. Blood was sampled and tissues collected and cleaned of excess blood and weighed for *ex vivo* analysis. Tumours were fixed for further analysis by immersion in 4% (w/v) paraformaldehyde in phosphate buffered saline. A Perkin Elmer 2480 Automatic Gamma Counter was used to measure radioactivity in tissues. The gamma counter was calibrated using known samples of ^{89}Zr and measured activity presented as

%ID/g based on injected activities. Figure S12 shows a comparison of targeted ($[^{89}\text{Zr}]\text{HBP3-A}$) and untargeted ($[^{89}\text{Zr}]\text{HBP3}$) nanomedicine *ex vivo* biodistribution at 9 days post injection.

Ex vivo nanomedicine biodistribution

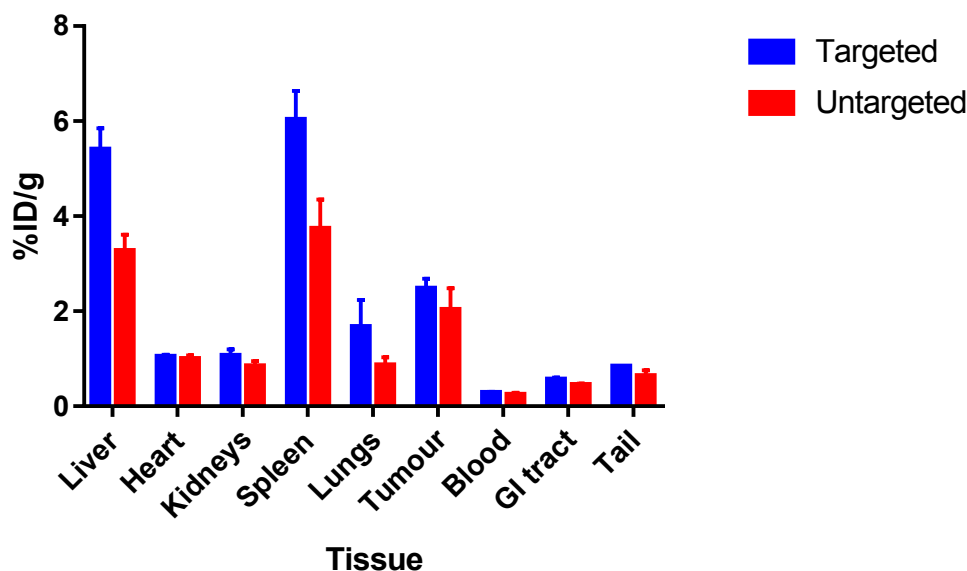


Figure S12 – Biodistribution of targeted and untargeted HBP 9 days post injection as measured by gamma counter

Confocal Microscopy of Ex Vivo Tumour Slices

Fixed tumours were then embedded in paraffin, sectioned into 100 μm slices, H&E stained and mounted onto slides for imaging. Fixed tumour slices from animals administered **HBP3-A** were examined using a Zeiss 710 laser scanning confocal microscope housed in the Australian National Fabrication Facility Queensland node. This microscope is equipped with argon, 405 diode and helium-neon lasers, in addition to 10x, 20x and 40x objectives. In H&E stained samples, connective and fibrous tissue (i.e.: collagen, elastin etc.) was excited at 405 nm, Evans blue at 561 nm and Cy5.5 labelled polymer at 633 nm being excited using sequential scanning; fluorescence was collected at 410-470 nm, 640-750 nm and 645-750 nm respectively. Images of the entire tumour slice were collected using the 10x objective, with images being stitched together; greater detail of features at the periphery and centre were garnered using the 20x objective and cellular level examination was performed using the 40x water immersion lens (Figure S13, Figure S13 and Figure 1C).

As described in the main body of the manuscript, **HBP3-A** polymer is observed towards the periphery of the tumour mass, rarely more than 100 μm away from blood vessels. Diffuse Cy5.5 fluorescence is also present in these regions with limited distribution through the core of the tumour (Figure S13-15). While small blood vessels are uncommonly scattered throughout the tumour volume (brighter green flecks), the majority occur at the tumour boundary, and are associated with higher levels of nanomedicine. In addition Figure S15 shows separate fluorescence channels of a portion of the tumour periphery illustrating localization of nanomedicine close to visible vasculature. Figure S16 then shows cellular level images of nanomedicine localization, suggesting that the visible aggregates are the result of uptake into cells.

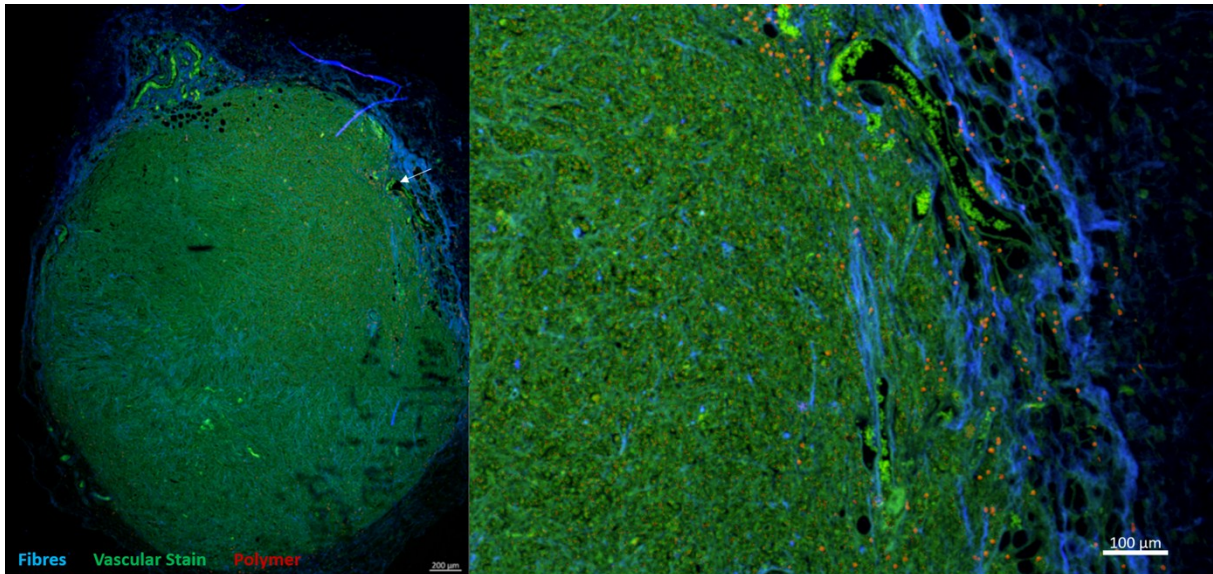


Figure S13 - Confocal microscopy images of tumour slice and higher magnification of the region marked with an arrow. H&E stain for collagen & connective fibres shown in blue, vasculature stain (Evans Blue) in green and polymeric nanomedicine HBP3-A in red.

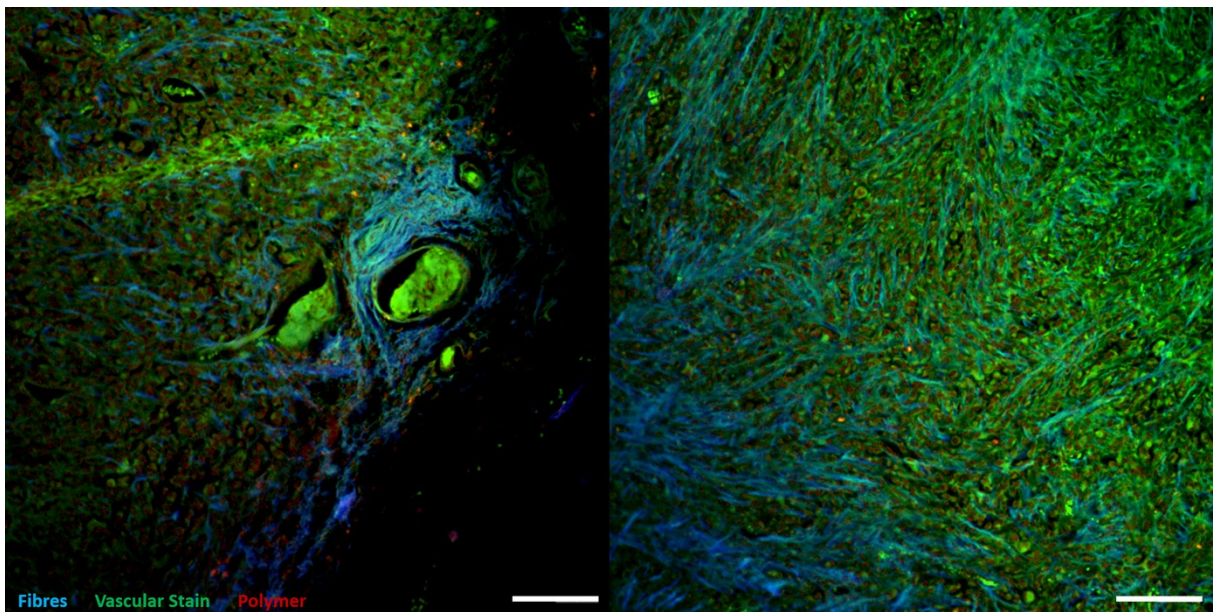


Figure S14 - Representative higher resolution confocal microscopy images of tumour periphery (left) and centre of tumour mass (right). Fluorescence channels coloured as in Figure S13. White scale bar equivalent to 100 µm. Separate fluorescence channels for the left image available in Figure S15.

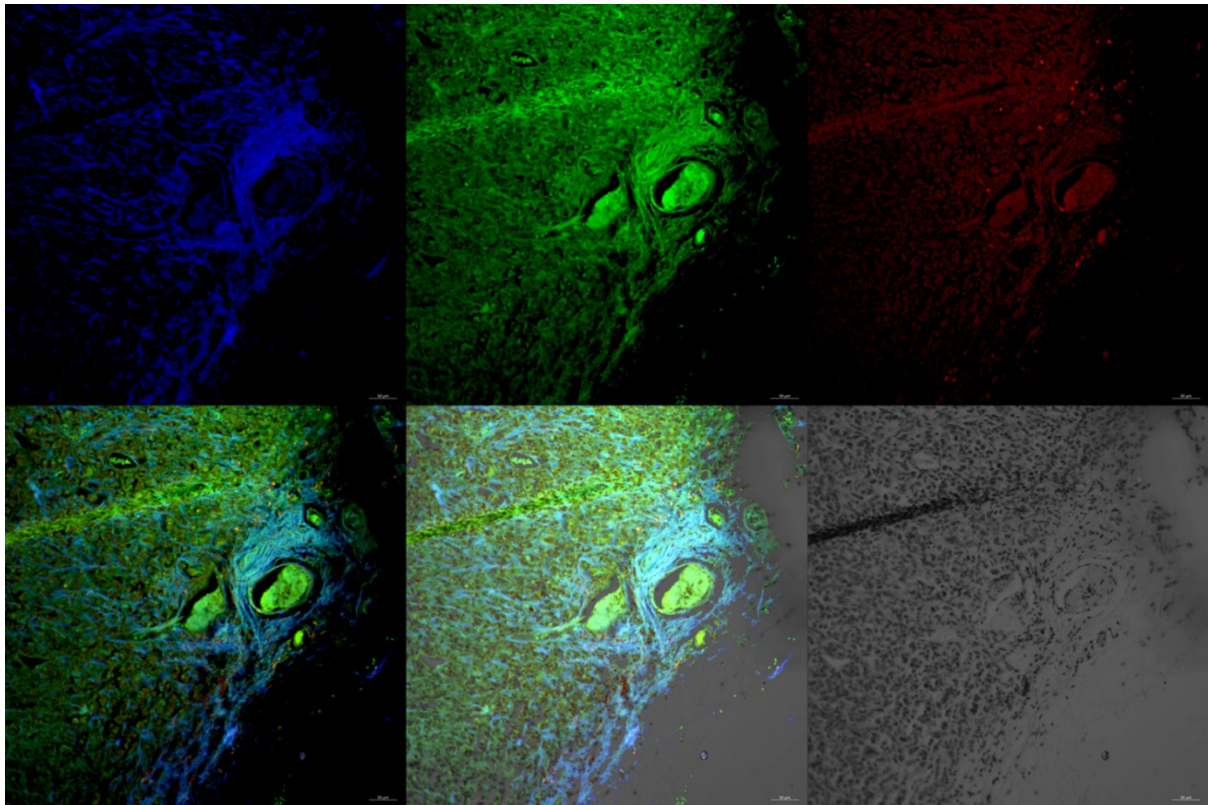


Figure S15 – Separate fluorescent channels acquired by confocal microscopy of a portion of the tumour periphery comprising several blood vessels. H&E stain for collagen & connective fibres shown in blue, vasculature stain (Evans Blue) in blue and polymeric nanomedicine HBP3-A in red

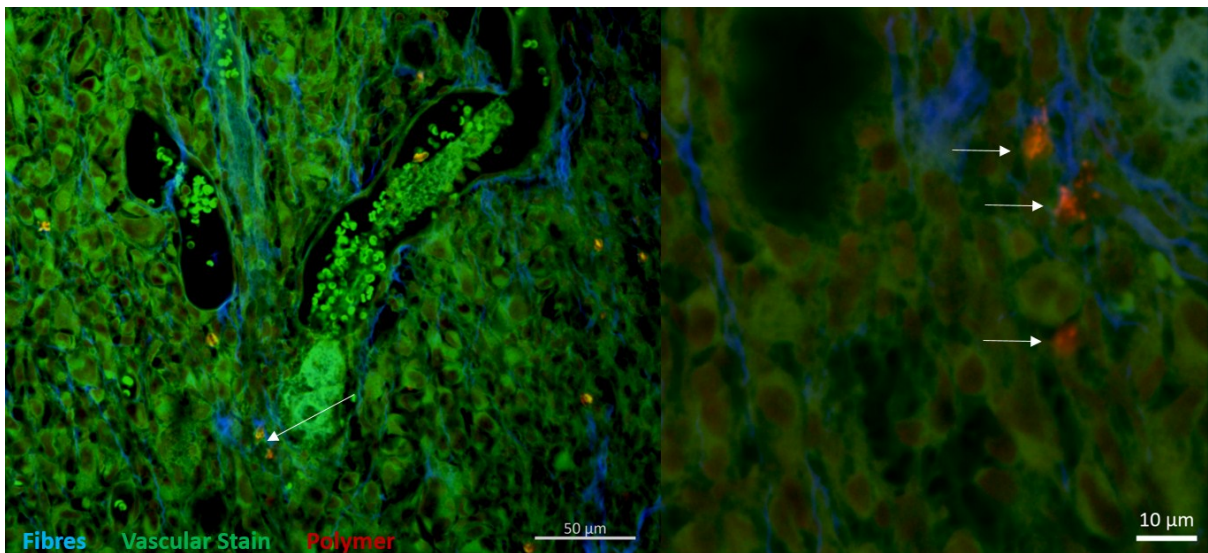


Figure S16 - Cellular level images of blood vessel and tumour cells, aggregation into cells marked with arrows.

References

1. A. Ardana, A. K. Whittaker and K. J. Thurecht, *Macromolecular Research*, 2017, **25**, 599-614.
2. A. K. Pearce, A. V. Fuchs, N. L. Fletcher and K. J. Thurecht, *Pharmaceutical research*, 2016, **33**, 2388-2399.
3. N. R. B. Boase, I. Blakey, B. E. Rolfe, K. Mardon and K. J. Thurecht, *Polymer Chemistry*, 2014, **5**, 4450-4458.
4. A. V. Fuchs, B. W. Tse, A. K. Pearce, M. C. Yeh, N. L. Fletcher, S. S. Huang, W. D. Heston, A. K. Whittaker, P. J. Russell and K. J. Thurecht, *Biomacromolecules*, 2015, **16**, 3235-3247.